20th European Wireless Conference

Bi-orthogonal Waveforms for 5G Random Access with Short Message Support

MARTIN KASPARICK[1], GERHARD WUNDER[1,2], PETER JUNG[1,2], DICK MARYOPI[1]

[1]Fraunhofer Heinrich Hertz Institute (HHI), Berlin, Germany
[2]Technische Universität Berlin, Germany

July 10, 2014

Abstract

One of the main drivers for new waveforms in future 5G wireless communication systems is to handle efficiently the variety of traffic types and requirements. In this paper, we introduce a new random access within the standard acquisition procedures to support sporadic traffic as an enabler of the Internet of Things (IoT). The major challenge hereby is to cope with the highly asynchronous access of different devices and to allow transmission of control signaling and payload "in one shot". We address this challenge by using a waveform design approach based on bi-orthogonal frequency division multiplexing. We show that this approach allows data transmission in frequencies that otherwise have to remain unused. More precisely, we utilize frequencies previously used as guard bands, located towards the standard synchronous communication pipes as well as in between the typically small amount of resources used by each IoT device. We demonstrate the superiority of this waveform approach over the conventional random access using numerical experiments.

5GNOW is a European research project supported by the European commission within FP7 ICT Call 8.
www.5gnow.eu

I. Introduction

The Internet of Things (IoT) is expected to foster the development of 5G wireless networks and requires efficient access of sporadic traffic generating devices. Such devices are most of the time inactive but regularly access the Internet for minor/incremental updates with no human interaction, e.g. machine-type-communication (MTC). Sporadic traffic will dramatically increase in the 5G market and, obviously, cannot be handled with the bulky 4G random access procedures [1].

The new conceptional approach in this paper is to use an extended physical layer random access channel (PRACH) which achieves device acquisition and (possibly small) payload transmission "in one shot". Similar to the implementation in UMTS, the goal is to transmit small user data packets using the PRACH, without maintaining a continuous connection. So far, this is not possible in LTE, where data is only carried using the physical uplink shared channel (PUSCH) so that the resulting control signaling effort renders scalable sporadic traffic (e.g., several hundred nodes in the cell) infeasible. By contrast, in our design a data section is introduced between synchronous PUSCH and standard PRACH, called *D-PRACH* (data PRACH) supporting asynchronous data transmission. E.g., in the simplest approach the D-PRACH uses the guard bands between PRACH and PUSCH. Clearly, by doing so, sporadic traffic is removed from standard uplink data pipes resulting in drastically reduced signaling overhead. Another issue that is closely related to the signaling overhead is the complexity and power consumption of the devices. We show that waveform design in such a setting is necessary since the OFDM waveform used in LTE cannot handle the highly asynchronous access of different devices with possible negative delays or delays beyond the cyclic prefix (CP). Clearly, guards could be introduced between the individual (small) data sections which, though, makes the approach again very inefficient. Moreover, giving up guard bands for transmitting data will naturally lead to increased interference for PUSCH users which must be also handled with waveform design.

We propose a bi-orthogonal frequency division multiplexing (BFDM) based approach [2][3], where we replace orthogonality of the set of transmit and receive pulses with bi-orthogonality. In particular, time-frequency representations of the transmit and receive pulses are pairwise (not individually) orthogonal. Thus, there is more flexibility in designing a transmit prototype, e.g., in terms of side-lobe suppression. However, instead of a matched filter an optimally mismatched filter will be used [2]. The BFDM approach is well suited to sporadic traffic, since the PRACH symbols are relatively long so that transmission is very robust to (even negative) time offsets. In addition, BFDM is also more robust to frequency offsets in the transmission which, as well-known, typically sets a limit to the symbol duration in OFDM transmission. Finally, the concatenation of BFDM and several OFDM symbols together requires a good tail behavior of the transmit pulse in order to keep the distortion to the payload carrying subcarriers in PUSCH small. Conversely, the dual pulse which accounts for the distortion of PUSCH onto PRACH can be controlled by iterative interference cancellation (if necessary). This alleviates the typical problem of controlling time/spectral localization of pulse and dual pulse. The excellent and controllable tradeoff between performance degradation due to time and frequency offsets is the main advantage of BFDM with respect to conventional OFDM.

We investigate the performance of the proposed approach using numerical experiments where, for comparison, a standard LTE system serves as a baseline. We show how the new approach can actually reduce the interference to the PUSCH region. Moreover, we demonstrate that the performance in the new D-PRACH region is significantly improved by the pulse shaping approach when multiple, completely asynchronous, users transmit data in adjacent frequency bands.

A. Organization

The paper is organized as follows. In Section II, we introduce the system model and the considered LTE channels. In Section III, we describe the proposed pulse shaped PRACH based on BFDM. In Section IV and Section V, we deal with the issues of user detection and channel estimation in the novel D-PRACH, respectively. In Section VI, we investigate the performance of the proposed approach numerically and compare to the standard LTE approach. In Section VII, we summarize the findings and draw important conclusions.

This work was carried out within the 5GNOW project, supported by the European Commission within FP7 under grant 318555, and within DFG grant JU-2795/2.

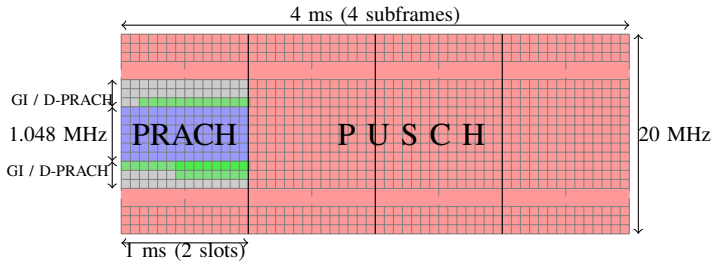

Fig. 1: PRACH (blue) and PUSCH (red) regions. A guard interval (GI) separates PUSCH from PRACH in LTE (gray). Parts of this area are used for data transmissions of asynchronous users (green) in a novel D-PRACH, whose size can be variably determined by MAC. Rows in this illustration do not represent true subcarrier quantities.

II. System Model and Notation

We consider a simple uplink model of a single cell network, where each mobile station and the base station are equipped with a single antenna. We assume there exist two channels–in LTE terminology–the PUSCH and the PRACH. On the PUSCH, the data bearing signals are transmitted from synchronized users to the base station using Single Carrier Frequency Division Multiple Access (SC-FDMA). A small part of the resources is reserved for PRACH, in which, at the first step of the RACH procedure, users send preambles that contain unique signatures. In this paper we mainly deal with the PRACH design, trying to leave PUSCH operations as unaffected as possible.

The time-frequency resource grid for the described channels is illustrated in Figure 1. To minimize the interference between the channels, several subcarriers on both sides of the PRACH are usually left zeros as a guard band. In this paper, however, we will exploit the PRACH to carry some data on the guard bands. These users, however, may be completely asynchronous which can be a serious challenge. Specific system parameters can be found in Table I or in LTE specifications [4]. Assuming an AWGN channel and one user transmitting its preamble signal on the PRACH, the base station obtains the superposition of data bearing signals, preamble signal, and noise as

$$r[n] = s_{\mathrm{PU}}[n] + s_{\mathrm{PR}}[n] + n_0[n], \tag{1}$$

where s_{PU} is the PUSCH data transmit signals, s_{PR} is the PRACH preamble transmit signal, and n_0 is Gaussian noise. In the following, let T_s denote the sampling period, which is equal to $1/f_s$, with f_s being the sampling frequency. Moreover, F denotes the subcarrier spacing. Furthermore, we use N to denote the discrete counterpart of the symbol duration. Let N_{FFT} be the FFT-length in PRACH.

III. Pulse shaped PRACH

We adopt a pulse shaping Bi-orthogonal Frequency Division Multiplexing (BFDM) scheme for PRACH transmissions. The underlying principle is to transmit the symbols according to a set of shifted pulses on time-frequency lattice points (kT, lF), where T is the time shift period and F is the frequency shift period and $k, l \in \mathbb{Z}$. As stated in [2], the only requirement of perfect symbol reconstruction is that the set of transmit pulses $\{g_{k,l}\}$ and the set of receive pulses $\{\gamma_{k,l}\}$ form bi-orthogonal Riesz bases. The determining factors to meet that condition are, first, the properties of the pulses itself, and second, the time-frequency product TF being greater than one. See also [5] for further explanation on these conditions. In this paper we choose $TF = 1.25$.

Let us now focus on transmitter and receiver design. Note that efficient implementations are available in literature [6][7].

A. Transmitter

For the pulse shaped PRACH, additional processing is needed, compared to standard OFDM. In contrast to standard processing, we process more than one symbol interval, even if we use only one symbol to carry the preamble. We refer to [3] for implementation details. A pulse g is used to shape the spectrum of the preamble signal (which is constructed from a Zadoff-Chu (ZC) sequence [8]), e.g., to allow the use of PRACH guard bands with acceptable interference. Let P be the length of pulse g. We extend the output signal $s[n]$ after the inverse FFT (IFFT) stage by repeating it and taking modulo P to get the same length as the pulse g. Given K symbols,

each symbol $s_k[n]$ is pointwise multiplied by the shifted pulse g and superimposed by overlap add, such that we get the base band pulse shaped PRACH transmit signal

$$s_{\mathrm{PR}}^{\mathrm{ps}}[n] = \sum_{k=0}^{K-1} s_k[n] g[n - kN]. \tag{2}$$

In greater detail, this can be written as

$$s_{\mathrm{PR}}^{\mathrm{ps}}[n] = \beta \sum_{k=0}^{K-1} \sum_{l=q}^{N_{\mathrm{ZC}}+m+q-1} \tilde{X}_{k,l}\, g[n - kN] e^{j\frac{2\pi nl}{N_{\mathrm{FFT}}}}, \tag{3}$$

where $\tilde{X}_{k,l}$ is the Fourier transformed ZC-sequence of length N_{ZC} at the k-th symbol and l-th subcarrier, q denotes the first subcarrier of the (extended) PRACH region, m is the guard band subcarriers occupied by messages, and β is an amplitude scaling factor for customizing the transmit power.

B. Receiver

The only difference to the standard PRACH receiver is the processing before the FFT. In standard PRACH processing, the cyclic prefix is first removed from the received signal $r_{\mathrm{PR}}[n]$ and then the FFT is performed. In the pulse shaped PRACH, an operation to invert the (transmitter side) pulse shaping has to be carried out first. To be more precise, the K symbols of the received signal $r_{\mathrm{PR}}[n]$ are pointwise multiplied by the shifted bi-orthogonal pulse γ, such that we have

$$r_k^{\gamma}[n] = r_k[n] \gamma^*[n - kN]. \tag{4}$$

Subsequently, we perform a kind of prealiasing operation to each windowed $r_k^{\gamma}[n]$, i.e.,

$$\tilde{r}_k^{\gamma}[n] = \sum_{l=0}^{P/N_{\mathrm{FFT}}-1} r_k^{\gamma}[n - lN_{\mathrm{FFT}}], \tag{5}$$

such that we obtain the Fourier transformed preamble sequence at the k-th symbol and l-th subcarrier after the FFT operation

$$\tilde{Y}_{k,l} = \sum_{n=0}^{N_{\mathrm{FFT}}-1} \tilde{r}_k^{\gamma}[n] e^{-\frac{j2\pi nl}{N_{\mathrm{FFT}}}}. \tag{6}$$

Although we do not employ a cyclic prefix as in standard PRACH, the time-frequency product of $TF = 1.25$ allows the signal to have temporal and frequency guard regions as well. This time-frequency guard regions and the overlapping of the pulses evoke the received signal to be cyclostationary [9], which gives the same benefit as the cyclostationarity made by cyclic prefix. Furthermore, it is also shown in [9], that the bi-orthogonality condition of the pulses is sufficient for the cyclostationarity and makes it possible to estimate the symbol timing offset from its correlation function.

C. Pulse Design

As mentioned before, the used pulses g and γ play a key role and should therefore be carefully designed. Since we consider here the BFDM approach, we setup the transmit pulse g according to system requirements and compute from g the receive pulse γ as the canonical dual (biorthogonal) pulse. For this computation we follow here the method already used, for example, in [5] (see also the further references cited therein). Briefly explained, bi-orthogonality in a stable sense means that g should generate a Gabor Riesz basis and γ generates the corresponding dual Gabor Riesz basis. From the Ron-Shen duality principle [10] follows that γ has the desired property if it generates on the so called adjoint time-frequency lattice a Gabor (Weyl-Heisenberg) frame which is dual to the frame generated by g. However, this can be achieved with the S^{-1}-trick explained in [11]. Side effects such as spectral regrowth due to periodic setting when calculating the bi-orthogonal pulses are negligible.

As a rough and well-known guideline for well-conditioning of this procedure, the ratio of the time and frequency pulse widths (variances) σ_t and σ_f should be approximately matched to the time-frequency grid ratio

$$\frac{T}{F} \approx \sqrt{\frac{\sigma_t}{\sigma_f}}, \tag{7}$$

and this should also be in the order of the channel's dispersion ratio [5]. However, here we consider only the first part (7) of this rule since we focus on a design being close to the conventional LTE PUSCH and PRACH.

We propose to construct the pulse g based on the B-splines in the frequency domain. B-splines have been investigated in the Gabor (Weyl-Heisenberg) setting for example in [12]. The main reason for using the B-spline pulses is that convolution of such pulses have excellent tail properties with respect to the L_1-norm, which is beneficial with respect to the overlap of PRACH to the PUSCH symbols. We also believe that they trade off well the time offset for the frequency offset performance degradation but this is part of further on-going investigations and beyond the conceptional approach here.

Because of its fast decay in time, we choose a second order B-spline (the "tent"-function) in frequency domain given by

$$B_2(f) = B_1(f) * B_1(f), \text{ where} \tag{8}$$

$$B_1(f) := \chi_{[-\frac{1}{2},\frac{1}{2}]}(f) \tag{9}$$

(and $*$ denotes convolution). It has been shown in [12] that $B_2(f)$ generates a Gabor frame for the (a, b)-grid (translating B_2 on $a\mathbb{Z}$ and its Fourier transform on $b\mathbb{Z}$) if (due to its compact support) $a < 2$ and $b \leq 1/2$ and fails to be frame in the region:

$$\{a \geq 2,\, b > 0\} \cup \{a > 0, 1 < b \in \mathbb{N}\}. \tag{10}$$

Recall, that by Ron-Shen duality [10] it follows that the same pulse prototype $B_2(f)$ generates a Riesz basis on the adjoint $(\frac{1}{b}, \frac{1}{a})$-grid. In our setting we will effectively translate the frequency domain pulse $B_2(f)$ by half of its support which corresponds to $\frac{1}{b} = \frac{3}{2}$ and we will use $\frac{1}{b} \cdot \frac{1}{a} = \frac{5}{4} = 1.25$ (see here also Table I) such that $a = \frac{6}{5}$. It follows therefore that our operation point $(a, b) = (\frac{6}{5}, \frac{2}{3})$ is not in any of two explicit (a, b)-regions given above. But for $1.1 \leq a \leq 1.9$ a further estimate has been computed explicitly for $B_2(f)$ [12, Table 2.3 on p.560] ensuring the Gabor frame property up to $b \leq 1/a$. Finally, we like to mention that for $ab \leq 1/2$ the dual prototypes can be expressed again as finite linear combinations of B-splines, i.e. explicit formulas exists in this case [13].

However, in practice g has to be of finite duration, i.e. the transmit pulse in time domain will be smoothly truncated:

$$g(t) = \left(\frac{\sin(B\pi t)}{B\pi t}\right)^2 \chi_{[c,d]}(t), \tag{11}$$

where B is chosen equal to F and parameters c and d align the pulse within the transmission frame. Theoretically, a (smooth) truncation in (11) would imply again a limitation on the maximal frequency spacing B [14]. Although the finite setting is used in our application, the frame condition (and therefore the Riesz-basis condition) is a desired feature since it will asymptotically ensure the stability of the computation of the dual pulse γ and its smoothness properties.

To observe the pulse's properties regarding time-frequency distortions we depict in Figure 2 the discrete cross-ambiguity function $A_{g,\gamma}$ between pulse g and γ which is given as:

$$A_{g,\gamma}(\tau, \nu) = \sum_n g[n]\gamma^*[n - \tau]e^{j2\pi\nu n}. \tag{12}$$

It can be observed, that its value at the neighboring symbol is already far below 10^{-3}. Obviously, the bi-orthogonality condition states $A_{g,\gamma}(kT, lF) = \delta_{k,0}\delta_{t,0}$ and ensures perfect symbol recovery in the absence of channel and noise. However, the sensibility with respect to time-frequency distortions is related to the slope shape of $A_{g,\gamma}$ around the grid points. Depending on the loading strategies for these grid points it is possible to obtain numerically performance estimates using, for example, the integration methods presented in [5].

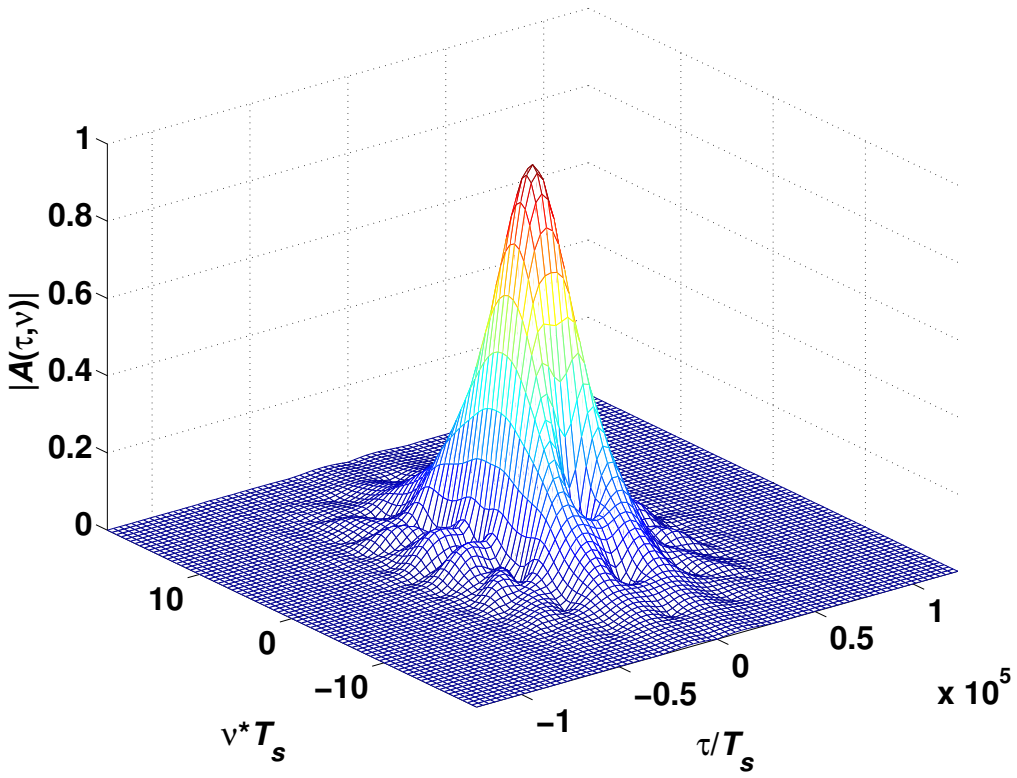

Fig. 2: The cross-ambiguity function $A_{g,\gamma}(\nu,\tau)$ for transmit and receive pulses on the frame length of $4\,\mathrm{ms}$.

IV. User Detection

A. Preamble generation

The preamble is constructed from a ZC sequence as

$$x_u[m] = \exp\left\{-j\frac{\pi u m(m+1)}{N_{\mathrm{ZC}}}\right\}, 0 \le m \le N_{\mathrm{ZC}} - 1, \tag{13}$$

where u is the root index and N_{ZC} is the length of the preamble sequence which is fixed for all users. We consider here the case of contention based RACH, where every user wanting to send a preamble chooses a signature randomly from the set of available signatures $\mathcal{S} = \{1, ..., 64 - N_{\mathrm{cf}}\}$, with N_{cf} being a given number of reserved signatures for contention free RACH. Every element of $\mathcal{S}$ is assigned to index (u, v), such that the preamble for each user is obtained by cyclic shifting the u-th Zadoff-Chu sequence according to $x_{u,v}[m] = x_u[(m + v\,N_{\mathrm{CS}}) \bmod N_{\mathrm{ZC}}]$, where $v = 1, ..., \left\lfloor \frac{N_{\mathrm{ZC}}}{N_{\mathrm{CS}}} \right\rfloor$ is the cyclic shift index and N_{CS} is the cyclic shift size. Since only $V = \left\lfloor \frac{N_{\mathrm{ZC}}}{N_{\mathrm{CS}}} \right\rfloor$ preambles can be generated from the root u, the assignment from $\mathcal{S}$ to (u, v) depends on N_{CS} and on the size of set $\mathcal{S}$.

B. Signature detection

Given the received signal (1), the PRACH receiver observes the fraction y that lies in the PRACH region to obtain the preamble. The receiver stores all available Zadoff-Chu roots as a reference. These root sequences are transformed to frequency domain and each of them is multiplied with the received preamble. As discussed in Section III-C, it approximately holds, as in OFDM,

$$Z_u[w] = Y[w]X_u^*[w], \tag{14}$$

where $Y[w]$ is the received preamble and $X_u[w]$ is the u-th ZC sequence in frequency domain respectively. Using the convolution property of the Fourier transform it is easy to show that $Z_u[w]$ is equal to the inverse Fourier

transform of any cross correlation function $z_u[d]$ at lag d. Because the preamble is constructed by cyclic shifting the Zadoff-Chu sequence, ideally we can detect the signature by observing a peak from the power delay profile, given by

$$|z_u[d]|^2 = \left| \sum_{n=0}^{N_{\mathrm{ZC}}-1} y[n+d]x^*[n] \right|^2 . \tag{15}$$

Let $N_{\mathrm{root}} = \left\lfloor \frac{64-N_{\mathrm{cf}}}{V} \right\rfloor$ be the number of roots that we require to generate $64-N_{\mathrm{cf}}$ preambles. Then, the signature S_i and the delay d_i of user i are obtained by $S_i = Vu + \left\lfloor \frac{\tau_l}{N_{\mathrm{CS}}} \right\rfloor$, $(0 \leq u \leq N_{\mathrm{root}})$ and $d_i = (\tau_l \bmod N_{\mathrm{CS}}) \times \frac{N_{\mathrm{FFT}}}{N_{\mathrm{ZC}}} T_s$, respectively, where τ_l is the location of the largest peak in (15).

V. Channel Estimation

The question remains how to obtain an estimation for the channel also on the new D-PRACH subcarriers. Due to our system setup, we assume that the received preamble signal can be written as

$$y = \underbrace{D \cdot W}_{\Phi} \cdot h + e. \tag{16}$$

Thereby, the term e accounts for all interference and noise, D is a diagonal matrix constructed from the coefficients of the Fourier transformed preamble and $W = F(\mathcal{I}_p, \mathcal{I}_h)$ is a sub-matrix of the $\mathbb{C}^{M\times M}$ DFT-matrix F. The set $\mathcal{I}_h := \{1, \ldots, n_h\}$ contains the indices of the first n_h columns, and $\mathcal{I}_p = \{i_1, \ldots, i_{N_{\mathrm{ZC}}}\}$ contains the indices of the central N_{ZC} rows of F. Furthermore, M is the length of the subframe without CP and guard interval, and we assume a maximum length n_h of the channel h.

For simplicity, we consider simple least-squares channel estimation, i.e., we have to solve the estimation (normal) equation $\Phi^H \Phi \hat{h} = \Phi^H y$. To handle cases where Φ is ill-conditioned, we use Tikhonov regularization. This popular method replaces the general problem of $\min_x \|Ax-y\|^2$ by $\min_x \|Ax-y\|^2 + \|\Gamma x\|^2$, with the regularization matrix Γ. In particular, for our model in (16)

$$\hat{h} = (\Phi^H \Phi + \Gamma^H \Gamma)^{-1} \Phi^H y \tag{17}$$

is used in place of the pseudo-inverse, where Γ has to be adapted to the statistical properties of e. We choose Γ to be a multiple of the identity matrix.

The idea behind the estimation approach is, that the estimated channel is also valid for subcarriers that are adjacent to the region that we actually estimate the channel for. Numerical experiments indicate that the MSE is smaller then 10^{-4} for up to 200 subcarriers outside of $\mathcal{I}_p$.

VI. Numerical results

In this section we verify, using numerical experiments, that using the PRACH guard bands to carry messages is indeed practicable. We compare the standard (LTE) PRACH implementation to our proposed spline pulse shaped PRACH.

A. Simulation Setup

The simulation parameters, chosen according to LTE specifications, are provided in Table I. For the computation of γ we use the LTFAT toolbox which provides an efficient implementation of the S^{-1}-trick [15]. Due to the properties of the pulses, and to fit the strict LTE frequency specification, we allow a small spillover effect from PRACH to PUSCH in time. Due to the PRACH pulse length of 4 ms, as depicted in Figure 1, we simulate the PUSCH over this time interval. Furthermore we use the maximal available LTE bandwidth of 20 MHz. In the LTE standard, the power of PRACH is variable and is incrementally increased according to a complicated procedure. To allow a meaningful comparison without having to implement to complete PRACH procedure, we choose the power of the PRACH such that approximately the same power spectral density as in PUSCH is achieved, as depicted in Figure 3. We simulate multipath channels with a fixed number of three channel taps. Moreover, we assume a maximum length of $n = 300$, which corresponds to a delay spread of roughly $5\,\mu$s, and which implies a maximum cell radius of 1.5 km. For the transmission in PRACH, we use 4-QAM modulation. Consequently, even in case the PRACH power is lower than in Figure 3, we still have the opportunity to reduce the modulation to BPSK.

TABLE I: System Specification

	PUSCH	standard PRACH	pulse shaped PRACH
Bandwidth	20 MHz	1.08 MHz	1.08 MHz
OFDM symbol duration	0.67 μs	800 μs	-
Subcarrier spacing F	15 kHz	1.25 kHz	1.25 kHz
Sampling frequency f_s	30.72 MHz	30.72 MHz	30.72 MHz
Length of FFT N_{FFT}	2048	24576	24576
Number of subcarrier L	1200	839	839
Cyclic prefix length T_{CP}	160 T_s 1st 144 T_s else	3168 T_s	0
Guard time T_g	0	2976 T_s	0
Pulse Length P	-	-	4 ms
Number of symbols K	14	1	1
Time-freq. product TF	1.073	1.25	1.25

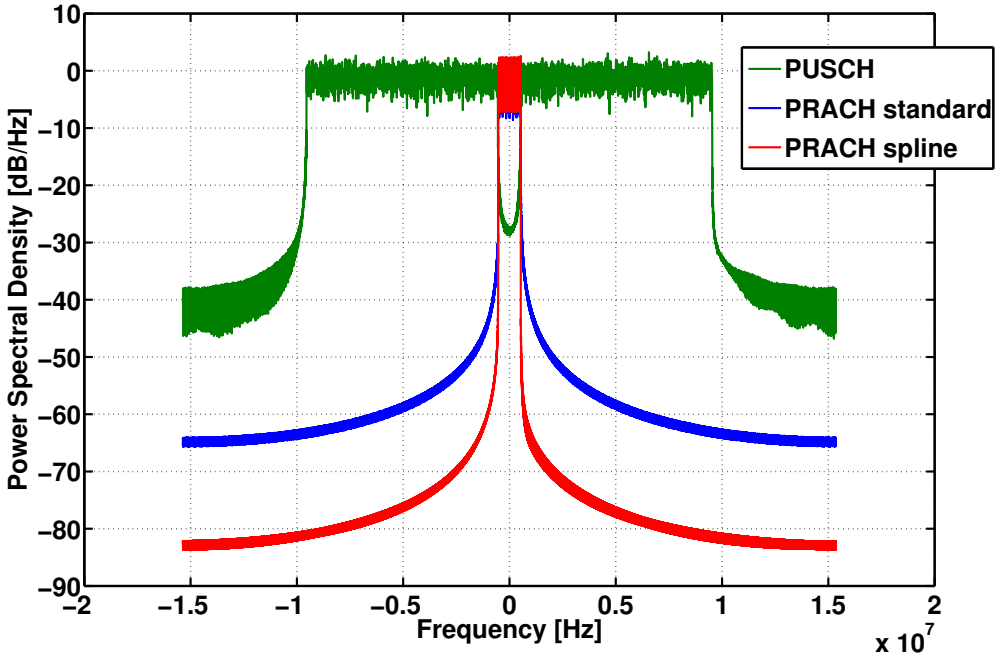

Fig. 3: Power spectral density. The power of the PRACH is chosen to achieve a similar PSD as PUSCH.

B. Data transmission in PRACH

Naturally, using the guard bands for data transmission causes an increased interference level in PUSCH. In Figure 4, we show the effect on PUSCH symbol error rate caused by data transmission on a variable number of D-PRACH subcarriers, given the standard LTE PRACH and the new BFDM-based PRACH approach. Clearly, the performance of PUSCH does not deteriorate due to the proposed BFDM-based PRACH. By contrast, irrespective of the actual number of subcarriers used for data transmission, the BFDM-based approach leads to a slightly reduced interference level in PUSCH. Due to the strong influence of the D-PRACH on neighboring subcarriers in PUSCH, this effect is stronger when no DFT-spreading is used in PUSCH. The reason why larger gains, which could be expected from Figure 3, cannot be realized is the PUSCH receiver procedure, which cuts out individual OFDM symbols from the received data.

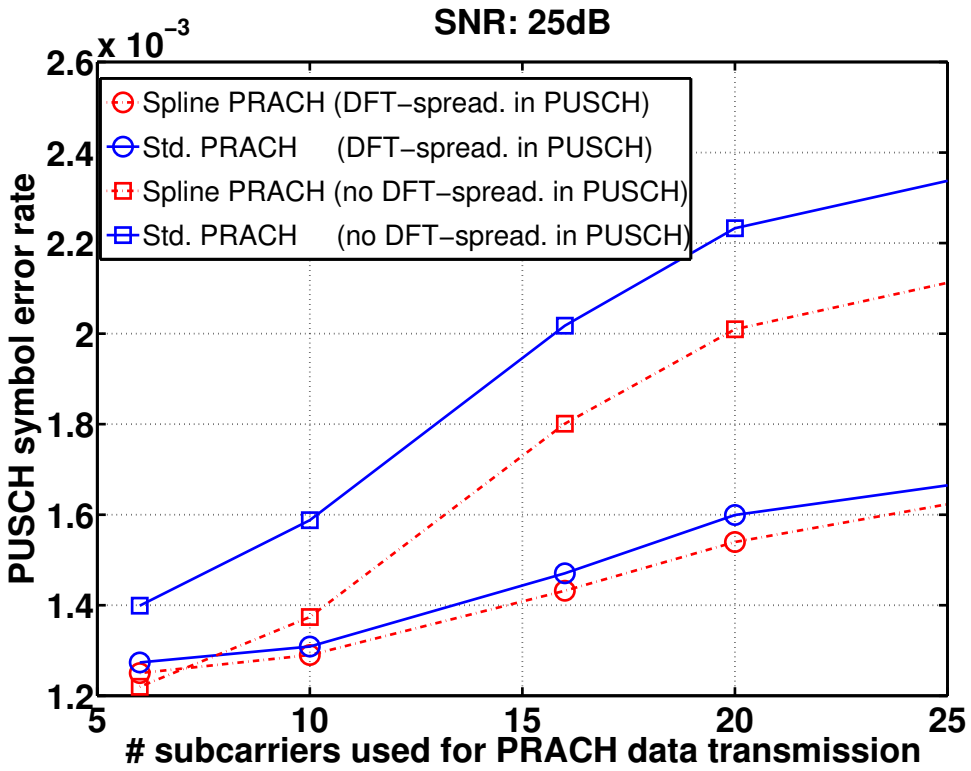

Fig. 4: Symbol error rate in PUSCH (averaged over all (1200) subcarriers) plotted over the number of D-PRACH subcarriers. The BFDM-based approach slightly reduces the symbol error rate. This effect is stronger when no DFT spreading is performed in PUSCH.

C. Asynchronous users

Asynchronous data transmission is a major challenge that comes with MTC and the Internet of Things. Therefore, we now consider a second, completely asynchronous, user that transmits data in the PRACH. Thereby we assign half of the subcarriers available for PRACH data transmission to this second user. However, we still evaluate only the performance of the original "user of interest" (and consequently we carry out channel estimation and decoding only for this user), which is assumed to transmit at the "inner" subcarriers close to the control PRACH. Thereby, we compare two waveforms, OFDM and the proposed spline approach. Figure 5 shows the results. We observe that for completely asynchronous users, i.e., offsets larger than the CP (in which case OFDM loses its orthogonality property), the new pulse shaped approach reduced the symbol error rate up to a factor of almost one half. Nevertheless, the resulting symbol error rate may still seem excessive. However, as Figure 6 shows, this effect can be compensated by allowing small guard bands (GB) in between the users. Figure 6 compares the performance of no GB and GBs of up to 4 subcarriers, which already drastically reduces the symbol error rate. Interestingly, the spline-based approach without GB achieves roughly the same performance as OFDM with a GB of 4 subcarriers. In other words, we can save 4 subcarriers using the spline-based PRACH.

VII. Conclusions

We proposed and evaluated a novel pulse shaped random access scheme based on BFDM, which is especially suited in random access scenarios due to very long symbol lengths. It turns out, that the proposed approach is well suited to support data transmission within a 5G PRACH. In particular, numerical results indicate that the BFDM-based approach does not deteriorate PUSCH operations, in fact, it even leads to a slightly reduced interference in PUSCH when using (previously unused) guard bands for data transmission, irrespective of the number of subcarriers used for data transmission. Even more importantly, completely asynchronous users, with time offsets larger than the cyclic prefix duration in standard PRACH, can be far better supported using the BFDM based approach than using

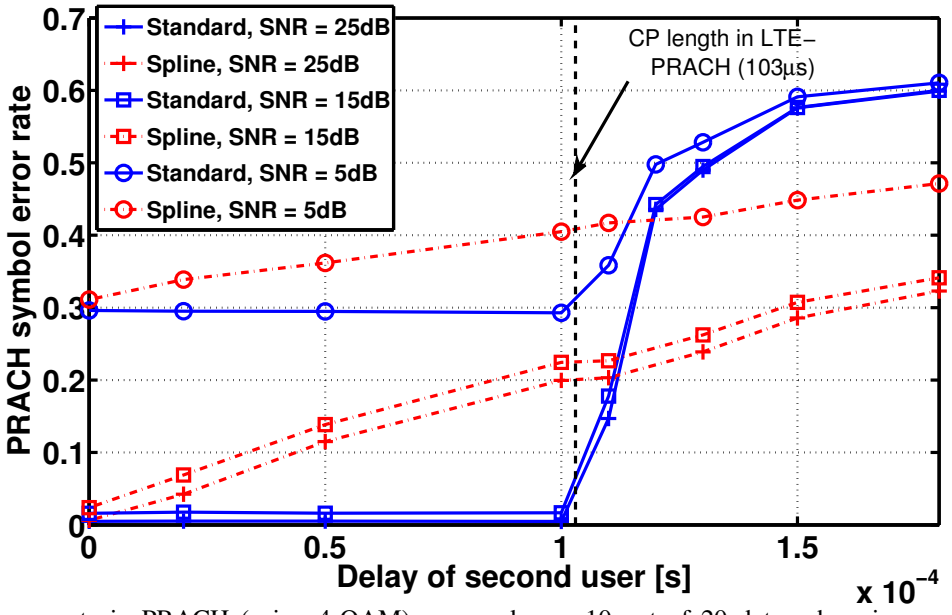

Fig. 5: Symbol error rate in PRACH (using 4-QAM) averaged over 10 out of 20 data subcarriers vs. the time offset of a second user. The other subcarriers are used by the second (asynchronous) user. The black line shows the CP length in LTE PRACH.

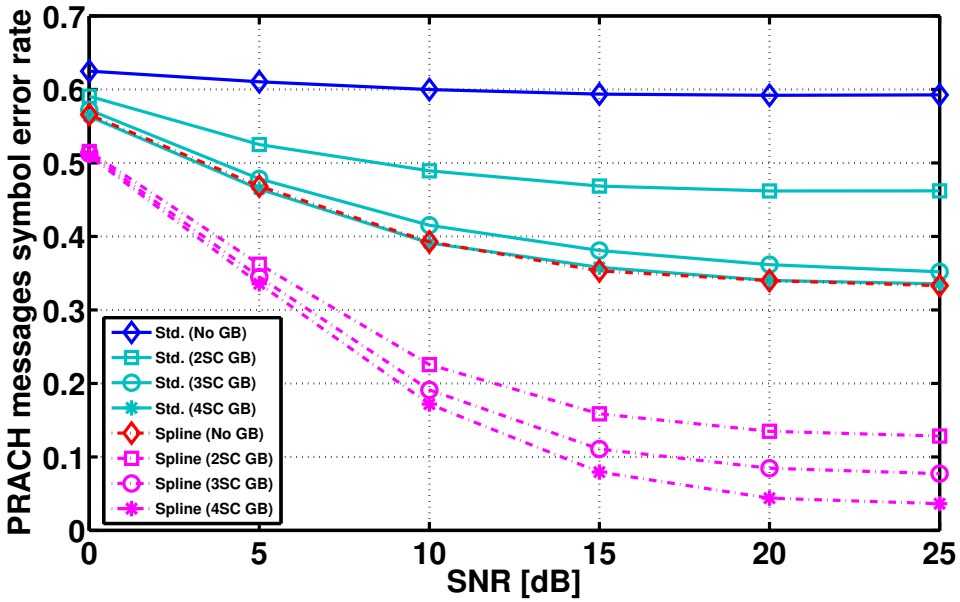

Fig. 6: Symbol error rate in PRACH (using 4-QAM) over SNR with presence of a second asynchronous user. Here, the second user has a time offset of 200 μs. The spline based approach outperforms OFDM with or without a small number of guard bands.

standard OFDM/SCFDMA. The presented results will help to cope with the upcoming challenges of 5G wireless networks and the Internet of Things, such as sporadic traffic.

REFERENCES

[1] G. Wunder, P. Jung, M. Kasparick, T. Wild, F. Schaich, Y. Chen, S. ten Brink, I. Gaspar, N. Michailow, A. Festag, L. Mendes, N. Cassiau, D. Ktenas, M. Dryjanski, S. Pietrzyk, B. Eged, P. Vago, and F. Wiedmann, "5GNOW: Non-Orthogonal, Asynchronous Waveforms for Future Mobile Applications," *IEEE Communications Magazine*, vol. 52, no. 2, pp. 97–105, 2014.

[2] W. Kozek and A. Molisch, "Nonorthogonal pulseshapes for multicarrier communications in doubly dispersive channels," *IEEE Journal Sel. Areas in Commun.*, vol. 16, no. 8, pp. 1579–1589, 1998.

[3] D. Schafhuber, G. Matz, and F. Hlawatsch, "Pulse-shaping OFDM/BFDM systems for time-varying channels: ISI/ICI analysis, optimal pulse design, and efficient implementation," in *13th IEEE International Symposium on Personal, Indoor and Mobile Radio Communications*, vol. 3, 2002, pp. 1012–1016 vol.3.

[4] S. Sesia, I. Toufik, and M. Baker, *LTE, The UMTS Long Term Evolution: From Theory to Practice*. Wiley Publishing, 2009.

[5] P. Jung and G. Wunder, "The WSSUS Pulse Design Problem in Multicarrier Transmission," *IEEE Trans. on Communications*, 2007.

[6] L. Vangelista and N. Laurenti, "Efficient implementations and alternative architectures for OFDM-OQAM systems," *IEEE Transactions on Communications*, vol. 49, no. 4, pp. 664–675, 2001.

[7] P. Jung and G. Wunder, "OQAM/IOTA Downlink Air Interface for 3G/4G," Fraunhofer MCI, Berlin, Tech. Rep., 2006.

[8] D. Chu, "Polyphase codes with good periodic correlation properties (corresp.)," *IEEE Transactions on Information Theory*, vol. 18, no. 4, pp. 531–532, 1972.

[9] H. Bolcskei, "Blind estimation of symbol timing and carrier frequency offset in wireless OFDM systems," *IEEE Transactions on Communications*, vol. 49, no. 6, pp. 988–999, 2001.

[10] A. Ron and Z. Shen, "Weyl–Heisenberg frames and Riesz bases in L_2(Rˆd)," *Duke Math. J.*, vol. 89, no. 2, pp. 237–282, 1997.

[11] I. Daubechies, "Ten Lectures on Wavelets," *Philadelphia, PA: SIAM*, 1992.

[12] V. D. Prete, "Estimates, decay properties, and computation of the dual function for Gabor frames," *Journal of Fourier Analysis and Applications*, 1999.

[13] R. S. Laugesen, "Gabor dual spline windows," *Applied and Computational Harmonic Analysis*, vol. 27, no. 2, pp. 180–194, Sep. 2009.

[14] O. Christensen, H. O. Kim, and R. Y. Kim, "Gabor windows supported on [-1,1] and dual windows with small support," *Advances in Computational Mathematics*, vol. 36, no. 4, pp. 525–545, 2012.

[15] P. Sondergaard, "Efficient Algorithms for the Discrete Gabor Transform with a Long FIR Window," *Journal of Fourier Analysis and Applications*, vol. 18, no. 3, pp. 456–470, 2012.